Carceller Candau, C.; Soto Pacheco, P.; Boria Esbert, VE.; Guglielmi, M.; Gil Raga, J. (2015). Design of Compact Wideband Manifold-Coupled Multiplexers. IEEE Transactions on Microwave Theory and Techniques. 63(10):3398-3407. doi:10.1109/TMTT.2015.2460738.

Design of Compact Wideband Manifold-Coupled Multiplexers

Carlos Carceller, *Member, IEEE,* Pablo Soto, *Member, IEEE,* Vicente Boria, *Senior Member, IEEE,* Marco Guglielmi, *Fellow, IEEE,* and Jordi Gil

***Abstract*—The design of manifold-coupled multiplexers for wideband applications is considered in this paper. A systematic procedure, based on the sequential connection of filters to the manifold and subsequent adjustment of the interconnection elements, is presented. The filters are attached to the manifold without using stubs, in order to minimize the effect of spurious resonances. The interconnection elements, the manifold and the remaining filters are considered as the first inverter of each new filter that is attached. This technique has been applied to several practical examples. The obtained results validate the proposed design methodology.**

***Index Terms*—Computer-aided design, multiplexing networks, resonator filters, wideband microwave components.**

I. Introduction

THE emergence and rapid development of modern communication systems has increased the demand for advanced microwave components. These modern devices must be capable of offering broad bandwidths, increased selectivity and high data rates while minimizing size, mass and production costs. In order to cope with increasingly tighter requirements, the complexity of such components has inevitably grown, where only highly optimized microwave devices are able to fulfill such stringent specifications. At the same time, shorter time-to-market goals put an important constraint on the efforts that can be devoted to the component design. First-time design success (this is, being able to design, build and succeed at the first attempt) is now highly sought after. Consequently, the demand for fast and accurate computer-aided design (CAD) methodologies has raised, in order to speed up the design process. Development of modern filters and multiplexers has been greatly benefited by this trend [1], [2].

Over the last four decades, extensive work has been published regarding the design of narrowband manifold-coupled multiplexers [3]–[10]. Given the sensitivity of these structures to manufacturing deviations, tuning elements are typically added and manually adjusted after fabrication to fulfill specifications. Hence, these type of multiplexers do not require an extremely accurate modeling of the different parts, since most deviations from ideal behavior can be accounted for by the final tuning process. Channel filters can be simply substituted by their equivalent models based on coupling matrices or lumped elements. Furthermore, a fundamental-mode characterization of the manifold and its junctions is accurate enough, in most cases, to achieve successful results [10].

Due to the narrow bandwidth of the filters involved, there are two effects that aid in the matching of all the filters in narrowband multiplexers. On the one hand, the interaction of one filter in the small passband of any other does not exhibit an important dependence with frequency. Therefore the manifold is able to provide a good matching for all channels. On the other hand, it is easy to implement the first inverter of each narrowband filter attached to the manifold, due to the low coupling level required. From the previous discussion it can be concluded that the interconnection of narrowband filters to a manifold-coupled multiplexer is not a severe issue. In fact, according to the usual design technique summarized in [1], the filters are connected to the manifold through half-wavelength stubs, and are separated along the manifold using near half-wavelength waveguide sections. The part of the multiplexer performing the interconnection has, therefore, many degrees of freedom which can be exploited to obtain a good matching of the different channels with only minor adjustments in the very first stages of each filter. To obtain such flexibility, the resulting interconnecting network (manifold and stubs) is normally long and bulky.

In contrast, design techniques for wideband multiplexers (in this paper, this term refers to those with a 20% relative bandwidth or higher) have been developed to a much smaller extent. A series of issues arise during the design of these wideband components. The main one is due to the interaction between the different filters and the manifold, which is much stronger than in the narrowband case. Undesired resonances are more troubling and must be avoided in a wider frequency range. Another issue involves the physical implementation of the input coupling for each filter. The coupling structure must provide the high coupling level required and, at the same time, compensate for the frequency-dependent loading effect of adjacent filters. These two issues become more troublesome as the number of channels increases. For that reason, most publications related to the design of wideband multiplexers are focused on diplexers [11]–[13]. As far as multiplexers are concerned, a manifold based on a cascade connection of Y-junctions for wideband applications has been proposed in [14] together with a tailored design technique. The solution requires interconnecting stubs and a bulky and intricate manifold (that can reduce the available coupling from the common port to the last channel filters). However, the component designed in [14] included only moderate bandwidth filters, whereas the

C. Carceller, P. Soto, V. Boria and M. Guglielmi are with Universitat Politecnica de Valencia, 46022, Valencia, Spain. Email: carcarc2@upvnet.upv.es, pabsopac@dcom.upv.es, vboria@dcom.upv.es

J. Gil is with Aurora Software and Testing S.L., Valencia, Spain.

This work was supported by the Spanish Ministerio de Economia y Competitividad under R&D project TEC2013-47037-C5-1-R.

frequency range covered by the entire multiplexer was not very wide.

In any case, there are applications that require multiplexers with a wide frequency band of operation. Classical narrowband manifold-coupled multiplexer design techniques are not suitable for this kind of applications. When designing wideband multiplexers, it is convenient to have a short manifold to avoid unwanted resonances in the frequency range of interest. Moreover, the stubs between filters and the manifold are particularly dangerous, since they can be an important source of these undesired resonances, and also accentuate the loading effect (and its variation with frequency) of each filter over the other channels. As it can be inferred, the proper connection of filters to the manifold is the main problem of a design methodology for wideband multiplexers. In this paper, a novel systematic and effective procedure to achieve this goal is presented. As explained in Section II, and in contrast with traditional techniques for multiplexer design, filters are sequentially connected to the manifold without the aid of stubs. The interconnection iris, but also the rest of the multiplexer, is considered as the first inverter of each filter to be attached. Although a similar concept was proposed in [15] for star-junction diplexers with limited filter interactions, in this work it is extended to manifold-coupled multiplexers. In addition, and thanks to the use of an iterative technique, it can also be applied to filters with strong interactions (which is the usual case for wideband multiplexers including moderate or wideband filters). The resulting new algorithm only requires the adjustment of a very reduced number of variables in each design step, and only the center frequency of each filter is considered at any given time. Consequently, the proposed methodology is simple and very efficient.

Section III includes several examples of multiplexers designed using the proposed methodology. As it will be shown, this methodology yields excellent results when compared with existing, more classical approaches. Measurements from two manufactured wideband multiplexers fully validate the proposed design methodology.

II. Connection of Filters to the Manifold

The manifold-coupled multiplexer configuration is considered in this paper. One end of the manifold contains either a filter or a short circuit, while the other end constitutes the common port (CP). Filters are spaced along the manifold and directly connected to it via H- or E-plane T-junctions. No stubs are located between the first coupling window of each filter and the manifold, as depicted in Fig. 1. The use of these additional stubs is widely adopted by multiplexer designers, mainly because it offers a simple way of increasing the degrees of freedom in the structure. Therefore, it is easier to achieve an adequate matching between filters and manifold without readjusting most of the filters dimensions (typically, only the first two resonators and couplings of each filter are modified). Compared with the classical configuration, the proposed connection of filters considered in this work leads to more compact designs. In addition, undesired resonances (which may interfere with other filters in the multiplexer) can be largely mitigated by removing such stubs.

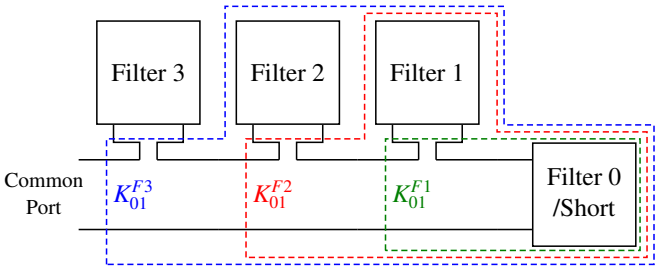

Fig. 1. Schematic of the sequential filter connection to the manifold.

Solutions to cope with unwanted spikes generated by the manifold were presented in [16]. They included reducing the height of the manifold waveguide and reducing the size of the coupling slots. The configuration proposed in this paper is compatible with making use of a reduced-height manifold, although additional effort must be done to design the transition from the common port to a standard waveguide. Furthermore, as the height of the manifold is reduced, so does the power handling capability of the multiplexer. Regarding the reduction of size in the coupling slots, this solution works for narrowband multiplexers. Otherwise, reducing the size of the input coupling slot is detrimental to the implementation of the high coupling values that wideband filters require for these particular slots. As an alternative, the authors in [17] cleverly proposed to take advantage of the unwanted resonances and used them as additional poles of the channel filter function. However, the extension of this technique to wideband multiplexers is not direct. The implementation in a wide frequency band of the input coupling and first resonator, by simply adjusting sections of transmission line, is a difficult task.

In this paper, a different approach is developed. The idea is to connect filters directly to the manifold, one by one. At each iteration, the spacing between the filter to be attached and the previous junction is adjusted, in order to achieve a strong coupling to the branching arm where the filter is connected. This also contributes to a reduction in size of the input irises, limiting unwanted interactions in the multiplexer. Once this length is set, the first coupling iris and resonator of the connected filter are adjusted, so the overall structure behaves (in magnitude and phase) like the first inverter of the stand-alone filter. To summarize, three dimensions are adjusted for each filter: the distance to the previous junction, the size of the first coupling iris and the length of the first resonator.

The idea of designing a junction to behave like the first inverter of a filter was already applied in [15] to the design of compact diplexers. In that work both filters are directly connected to a star-junction. The design of the junction is driven by formulas based on the value of the first K inverter extracted from each filter. A basic condition for the application of these formulas is that the interaction between both filters of the diplexer must be close to zero, measured from the first resonator. This condition was verified using narrowband filters with passbands located far apart, but its suitability for other applications is questionable, especially in the case of wideband filters. In addition, the technique in [15] limits its

scope to star-junction multiplexers, since it does not define a way to separate the filters if a manifold waveguide were to be employed. In contrast, the methodology proposed in the current work determines the physical distance between filters in the manifold, and does not require filters to have great mutual isolation. Therefore, it can be applied to both contiguous and non-contiguous multiplexers.

As it will be seen, the proposed methodology does not avoid the need for an optimization of the multiplexer. Instead, it is able to provide a good initial point for the trickiest part of the design: the adjustment of the manifold and the first variables of each filter dominating the multiplexer interactions. Starting from this point, conventional design procedures, based on a sequential adjustment of the multiplexer on a filter-by-filter [1] or cavity-by-cavity [5] basis, can be applied.

The design procedure consists of several cycles. In the first cycle, each filter is sequentially connected to the manifold. After that, there may be additional cycles that sequentially readjust the variables governing the connection of each filter, while keeping the rest attached to the manifold.

A. First cycle

The first cycle of the design procedure can be described in three steps that are repeated until all filters are connected to the manifold. A flowchart for this first cycle is shown in Fig. 2.

Step 1: First, the physical length of transmission line l_n that separates the T-junction of filter n from the previously-connected network N_{n-1} has to be determined. N_{n-1} contains the section of the multiplexer that has already been adjusted in previous steps, namely, all filters from $n-1$ to 0 and the corresponding part of the manifold attached to them. As mentioned before, N_0 may either be a filter (connected in-line with the manifold) or a short-circuit. The physical structure used in this first step to determine l_n is depicted in Fig. 3, where Port 1 corresponds to the manifold (towards the common port) and Port 2 is the arm where filter n will be directly connected.

Classical multiplexer design calls for an initial separation between filters that is a multiple of half the manifold wavelength. It is assumed that the locations providing maximum field within the manifold are barely affected by the connection of the filters. In narrowband cases, where the input coupling is small, this may be an adequate assumption. However, as the input coupling increases, the coupling windows have a stronger effect in the field distribution along the manifold. For that reason, it is important to use EM models in determining the optimal value of l_n. Otherwise, the manifold may not be able to couple enough energy to the corresponding filter, particularly for a wide passband channel. The optimal value of length l_n is the one that minimizes the return loss from Port 2 (see Fig. 3) at the filter center frequency f_n. If the dimensions of Port 2 are the same as those of the input/output port of the channel filter, the minimum value of $|S_{22}|$ gives an indication of the maximum normalized impedance inverter parameter $\overline{K}$ that can be achieved by adjusting the coupling iris.

In a lossless design, given the fundamental-mode scattering parameters $\mathbf{S}'$ of the T-junction as well as the reflection

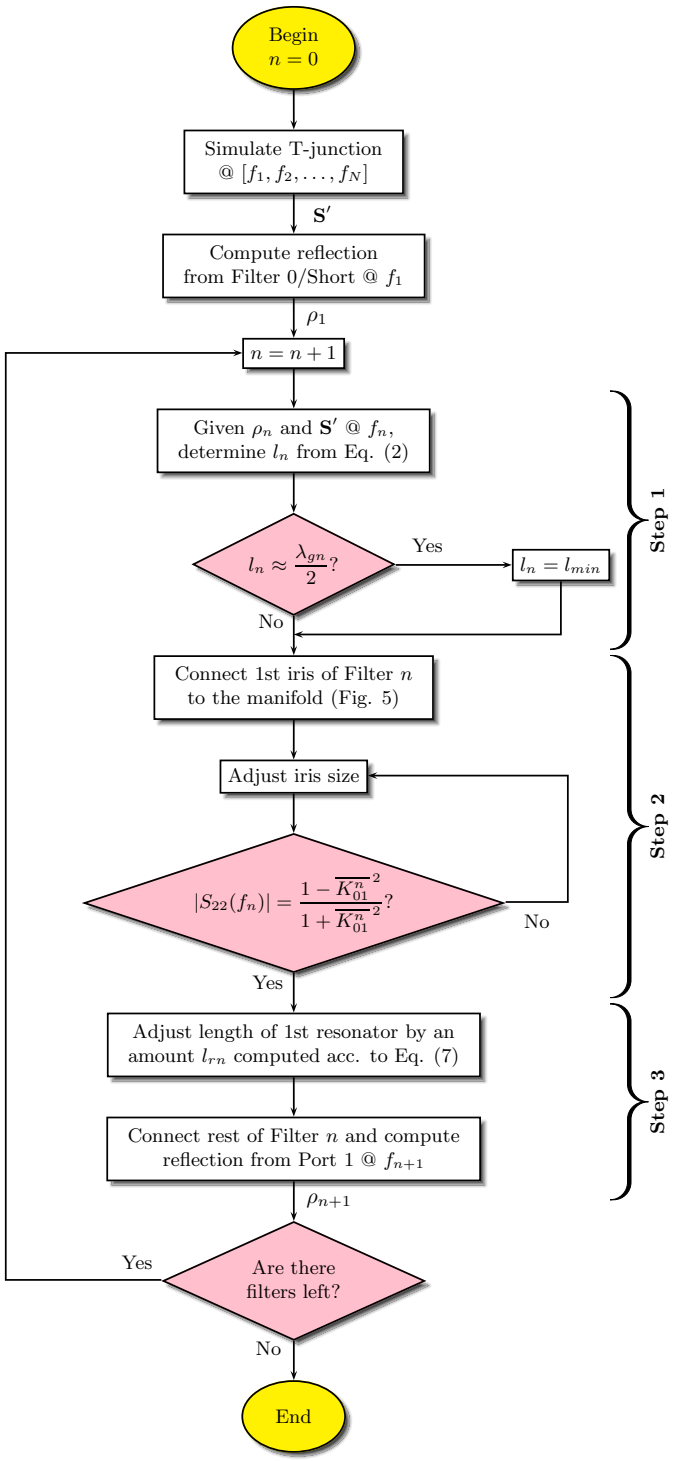

Fig. 2. Detailed flowchart summarizing the first cycle of the design procedure. This cycle starts with all the filters independently designed and sequentially connects them to the manifold.

coefficient ρ_n from the previously connected network, the return loss at Port 2 of Fig. 3 can be expressed as:

$$S_{22} = S'_{22} + \frac{S'^2_{23}\,\rho_n\, e^{-2j\beta_n l_n}}{1 - S'_{33}\,\rho_n\, e^{-j2\beta_n l_n}} \tag{1}$$

where β_n is the manifold phase constant at f_n.

An analytical solution for the length l_n that minimizes the

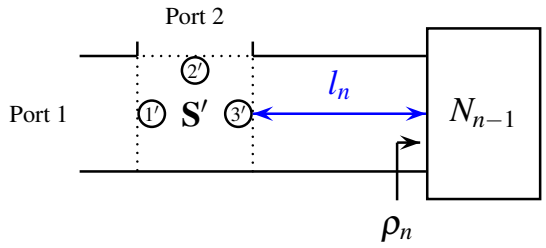

Fig. 3. Schematic of the structure used to adjust the spacing between junctions for filter n. Circled numbers indicate the reference port numbers for $\mathbf{S}'$.

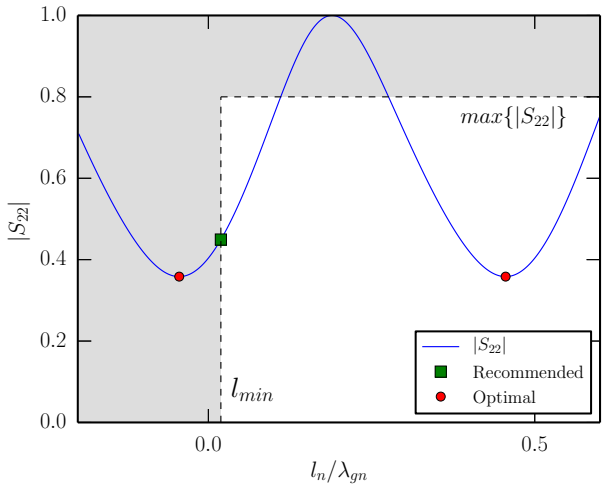

Fig. 4. Case example where the recommended length l_n differs from the optimal. Magnitude of the S_{22} parameter is depicted as a function of length l_n, normalized by the manifold wavelength. The shaded area defines the region where the normalized length is too small to fulfill mechanical specifications or the magnitude of $|S_{22}|$ is not low enough to implement the first inverter value (in this particular example, $\overline{K}_{01} = 0.33$).

reflection at Port 2 when $|\rho_n| = 1$ was proposed in [18]. As mentioned earlier, in wideband and contiguous multiplexers there can be a stronger interaction between filters. For that reason, the more general case where ρ_n can take any value is considered here for the first time. The optimal length l_n is:

$$l_n = \frac{\varphi_n - \psi + 2m\pi}{2\beta_n} \tag{2}$$

where φ_n is the phase of ρ_n, m is an integer value and phase ψ is computed as:

$$\psi = 2\tan^{-1}\left(\frac{B + \sqrt{A^2 + B^2 - C^2}}{A + C}\right). \tag{3}$$

Parameters A, B and C are extracted from $\mathbf{S}'$ and ρ_n:

$$\begin{aligned} A &= a_{33}\left(a_{22}^2 + a_{11}^2\,|\rho_n|^2\right)\sin\phi_{33} \\ &+ a_{11}\,a_{22}\left(1 + a_{33}^2\,|\rho_n|^2\right)\sin\left(\phi_{11} + \phi_{22} - \phi_s\right) \\ B &= a_{33}\left(a_{22}^2 + a_{11}^2\,|\rho_n|^2\right)\cos\phi_{33} \\ &- a_{11}\,a_{22}\left(1 + a_{33}^2\,|\rho_n|^2\right)\cos\left(\phi_{11} + \phi_{22} - \phi_s\right) \\ C &= 2\,a_{11}\,a_{22}\,a_{33}\,|\rho_n|\,\sin\left(\phi_{11} + \phi_{22} + \phi_{33} - \phi_s\right) \end{aligned} \tag{4}$$

where a_{ii} and ϕ_{ii} are, respectively, the magnitude and phase of the S'_{ii} parameter of the T-junction, and ϕ_s is the phase of the determinant of $\mathbf{S}'$.

As (2) shows, multiple solutions for l_n can be found, separated by half the manifold wavelength λ_{gn}. The greater length l_n is, the more troublesome the presence of spurious resonances becomes. In addition, the operational bandwidth of the T-junction decreases as l_n increases. Consequently, the smaller positive value of l_n that meets the physical and mechanical constraints of the multiplexer is selected. Occasionally, one of the solutions given by (2) may be very close to $\lambda_{gn}/2$. In those cases, it is suggested to use a non-optimal solution to avoid unwanted resonances. A length value closer to the minimum separation between filters that fulfills all mechanical constraints l_{min} could be chosen, as depicted in Fig. 4. Certainly, this solution can only be used as long as it is able to provide enough coupling for the implementation of the first inverter. Otherwise, the optimal but longer solution should be adopted.

In any case, the optimal solution provided by (2) is usually a good approximation to the desired solution for l_n. Since for wideband multiplexers the filters can be placed close to each other, the interaction between them could involve the fundamental mode but also higher-order modes. For that reason, it is recommended to perform a final refinement of l_n based on full-wave EM simulations. Once the EM-based solution for l_n is found, the aforementioned rule regarding solutions that are close to $\lambda_{gn}/2$ must also be applied.

Step 2: After setting the appropriate separation between filters, the first coupling iris is connected directly to the manifold (see Fig. 5). The iris is placed at the center of what is marked as Port 2 in Fig. 3. The size of this iris is then adjusted until the behavior of the structure at f_n is equivalent to the first inverter of filter n. The equivalent $\overline{K_{01}^n}$ inverter value is obtained from the full-wave simulation of the first iris of filter n as:

$$\overline{K_{01}^n} = \sqrt{\frac{1 - |\rho_{\text{iris}}(f_n)|}{1 + |\rho_{\text{iris}}(f_n)|}} \tag{5}$$

where ρ_{iris} is the reflection coefficient of the first iris detached from the rest of the filter. The iris size can be manually adjusted or an automatic optimization procedure can be launched until the magnitude of S_{22} is:

$$|S_{22}(f_n)| = \frac{1 - \overline{K_{01}^n}^2}{1 + \overline{K_{01}^n}^2}. \tag{6}$$

Step 3: Once the dimensions of the first iris are adjusted, the structure yields the same $|S_{22}|$ as the first coupling element of the original filter. However, the phase of S_{22} (φ_{22}) does not equal the phase of the first coupling element. Comparing φ_{22} with the objective phase $\varphi_{22}^{\text{obj}}$ of the original first coupling element, a certain length of transmission line l_{rn} is added to the filter first resonator. Generally, this length is negative, so it will be automatically absorbed by the resonator. It can be computed as:

$$l_{rn} = \frac{\varphi_{22} - \varphi_{22}^{\text{obj}}}{2\beta'_n} \tag{7}$$

where β'_n is the phase constant of the waveguide that implements the first resonator of the filter (i.e. the waveguide connected to Port 2 of Fig. 5) at frequency f_n.

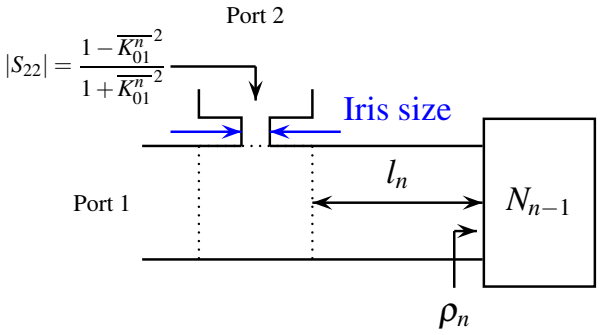

Fig. 5. Schematic of the structure used to adjust the size of the first coupling element of filter n in order to match the first inverter of the stand-alone filter. Dotted line indicates the reference plane of the T-junction with all ports having the same size, as shown in Fig. 3.

Finally, the remainder of the filter (second and subsequent resonators and coupling elements) is attached to the structure without altering its dimensions. This procedure is repeated until all filters are connected to the manifold. Note the simplicity (and therefore efficiency) of the proposed algorithm, since only three variables are adjusted in a sequential manner for each filter.

The order in which filters are connected to the manifold has an important effect in the performance of a wide-band multiplexer. With our proposed methodology, by the end of the first cycle (when all filters are connected to the manifold) the designer is able to spot potential problems in terms of spikes or insufficient coupling levels from the manifold to one of the filters. Since this methodology is very cost-effective, the designer can rearrange the filters in a different order and run the process once again, to see if problems have disappeared or there are additional benefits associated with the new arrangement.

Once this first cycle has ended, the response from the output port of the last filter connected must be very similar to the return loss of the stand-alone filter at its central frequency. During the first cycle, the effect that filter $n-1$ had on filter n was considered when adjusting the latter, but the opposite was not taken into account. For that reason, at least an additional design cycle must be run.

B. Additional cycles

In the following cycles, all filters must be connected to the manifold and the separation between filters is kept fixed (the field distribution in the manifold, starting from the short or filter 0, will not normally experience a severe change). The first coupling iris and first resonator length of each filter are sequentially readjusted to match the response of the corresponding first inverter of the isolated filter. Basically, the additional cycles consists on repeating Step 2 and Step 3 of the flowchart in Fig. 2 until all filters are adjusted. The difference with the first cycle is that now all filters (with the exception of the one that is being adjusted) are simultaneously connected to the manifold. In the first cycle, though, only the filters that had been previously adjusted were connected to the manifold.

The number of additional design cycles depends on the particular structure. Normally after the second or third complete cycle, the benefits in terms of response improvement does not justify the time spent on an additional iteration (in fact, sometimes the results start to oscillate after each cycle, meaning that this simple procedure has reached its limit). In general, this methodology tends to benefit the last filter readjusted, in the sense that it mainly improves the response of the multiplexer in this filter passband. As a result, the last cycle should not be fully completed, instead it must end after readjusting the most poorly matched filter (this is often filter 1 since it normally has the worst loading effect from the rest of the multiplexer).

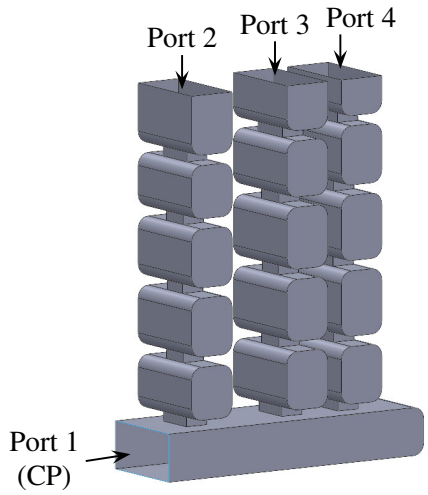

Fig. 6. Triplexer with rounded corners used to illustrate the design procedure.

III. Application Examples

In the following section, a series of manifold-coupled multiplexers are designed to validate the proposed design methodology.

A. Triplexer with rounded corners

The first example illustrates the design procedure explained in Section II through the simple design of the triplexer shown in Fig. 6. The three channel filters of order 4 are centered at 36.5 GHz, 38 GHz and 39.5 GHz, respectively, with 1 GHz bandwidth and 25 dB return losses. They are directly connected to the short-circuited manifold by their inductive irises. In addition, the presence of rounded corners, which typically appear when components are fabricated by milling, has been explicitly considered in the whole structure, including also the short-circuit at the end of the manifold (see Fig. 6). The relative bandwidth of the three filters is slightly above 2.5% but, overall, the relative bandwidth of the multiplexer is 10%. Although it is not a wideband example, but one with a moderate bandwidth, it is useful to clarify and understand the design steps. Furthermore, its simple topology enables the comparison of this method with existing ones proposed in the literature.

The connection of the filters to the manifold follows the guidelines described in Section II. Starting from the lower frequency filter, each one is sequentially connected to the

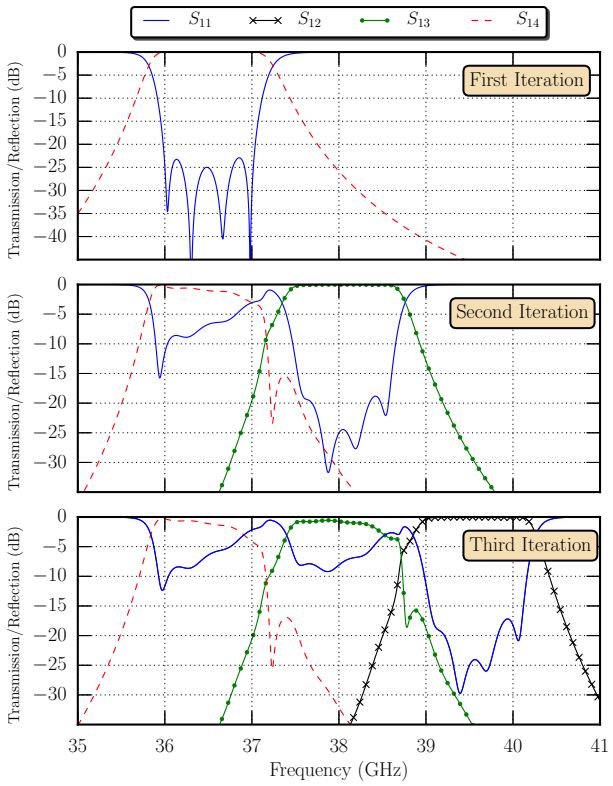

Fig. 7. Magnitude of the scattering parameters of the triplexer in Fig. 6, after each filter is assembled into the manifold and dimensions of the first iris and resonator are adjusted.

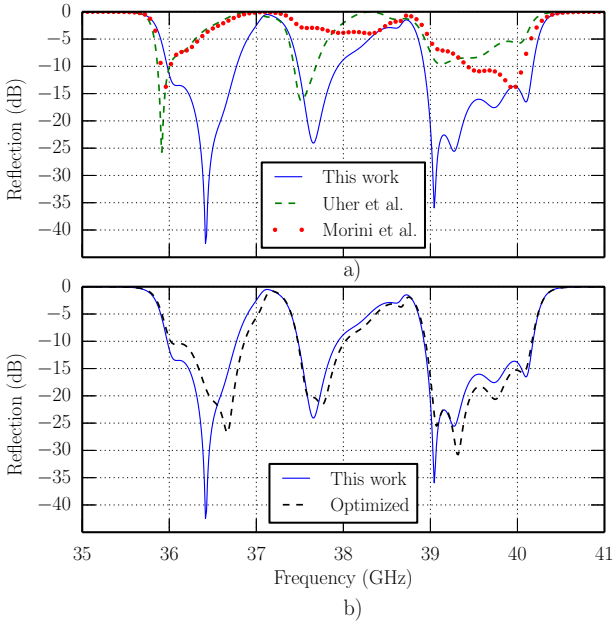

Fig. 8. Magnitude of the reflection coefficient at the common port of the triplexer with rounded corners after application of the design method. This initial response (solid line) is compared with alternative design procedures. a) Dashed line is obtained by connecting the filters directly to the manifold and separating them according to the expressions of [19]. Dotted line is obtained by spacing the filters according to [18] and adjusting the first coupling irises to fit formulae in [15]. b) Dashed line: response after a global optimization of the first stages (iris and resonator) of the triplexer.

manifold and its first iris and resonator adjusted. Figure 7 depicts the evolution of the reflection coefficient from the common port at the end of the first three iterations. On the first iteration, the adjusted manifold behaves similarly to the first inverter of filter 1 in most of its passband. Therefore, the common port return loss (CPRL) parameter of the multiplexer is almost equivalent to the return loss of the stand-alone filter, as can be seen in the "First Iteration" case of Fig. 7.

Once a second filter is added, though, the mutual loading between filter 1 and filter 2 deteriorates the response in both passbands. For filter 1 this implies that the first iris no longer behaves like the first inverter of the filter, thus the matching of the structure within its passband is worse than in the first iteration. Even if the matching is far from ideal, all four poles are still visible. As for filter 2, the response at its center frequency is recovered thanks to the adjustment of the first iris and resonator. Within its passband, however, the variation of the reactance of the previous filter (i.e. filter 1) is not smooth. This affects how well filter 2 can be matched with the rest of the multiplexer. Around the center frequency, the filter is considerably well matched, but closer to the edges of the passband the response is very different from its stand-alone version. Nevertheless, the return losses are better than 12 dB in the whole passband. Similarly, by the end of the third iteration (see Fig. 7), filter 3 is considerably well matched, whereas the matching of filters 1 and 2 has been deteriorated. It is worth noting that all poles can still be identified.

After the third iteration, two additional cycles are run (as mentioned in Section II, the last filter adjusted is filter 1). The eventual response obtained after application of the design technique is shown in Fig. 8 (solid line). This response is compared with two classical techniques for the initial design of multiplexers. In both cases the filters are directly connected to the manifold. In the first case, labeled "Uher et al.", filters are separated along the manifold according to the formulas in [19] and the first couplings are not changed. In the other case, labeled "Morini et al.", the design method of [15] is applied. Since [15] is focused on diplexers using star-junctions (rather than a manifold), the equations included in it cannot be exactly extrapolated to this example. Instead, the formulas of [18] are used to separate the filters along the manifold. Once this is done, the design criteria defined in [15] is applied to adjust the first coupling window and resonator of each filter. In contrast with our proposed methodology, the remaining filters are not connected to the manifold while adjusting the dimensions of each input iris. Thus, mutual filter interactions from the first resonators are being neglected. As can be seen in Fig. 8a, the two classical techniques yield similar results, whereas our proposed methodology considerably improves the initial multiplexer response. The availability of a better starting point guarantees a more efficient design of the whole multiplexer.

In order to test the performance of our method, an alternative solution has been considered as well. It has been obtained by optimization of the first iris and resonator of each filter using the simplex method. The separation between filters, though, has been fixed to the same value as our proposed initial design. The optimization goals have been set to achieve

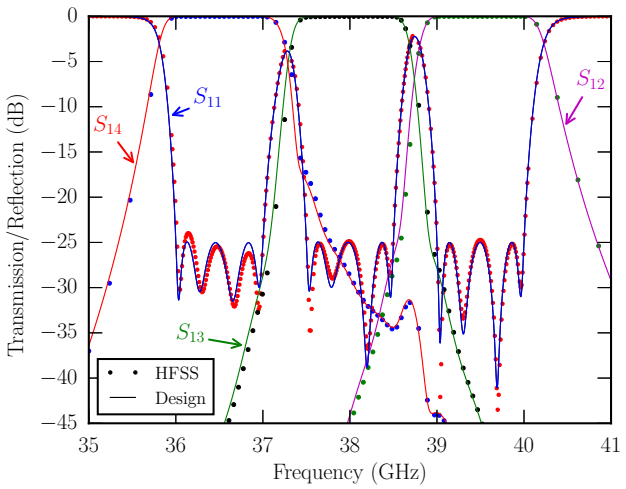

Fig. 9. Magnitude of the scattering parameters of the triplexer with rounded corners after optimization. This final design is successfully compared with the commercial software tool Ansys' HFSS 15.

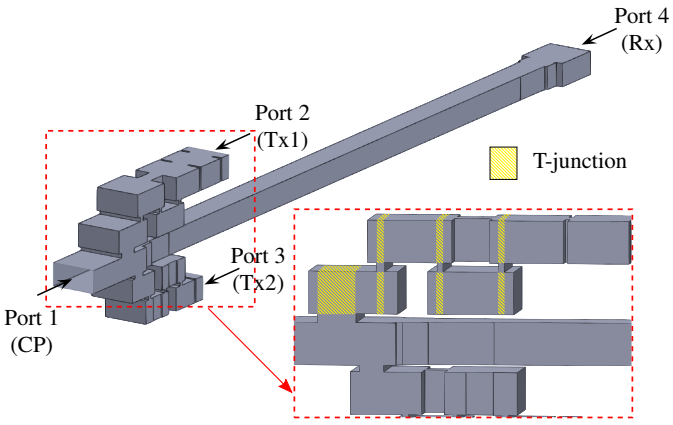

Fig. 10. Prototype of the triplexer for PIM measurements at Ku-band and detail of one of the filters. T-junctions are used to model the capacitive couplings of the HFRW filters, some of them placed close to inductive steps and therefore requiring a full-wave representation. Hatched areas in the detail of the figure indicate the T-junction blocks for the Tx1 filter.

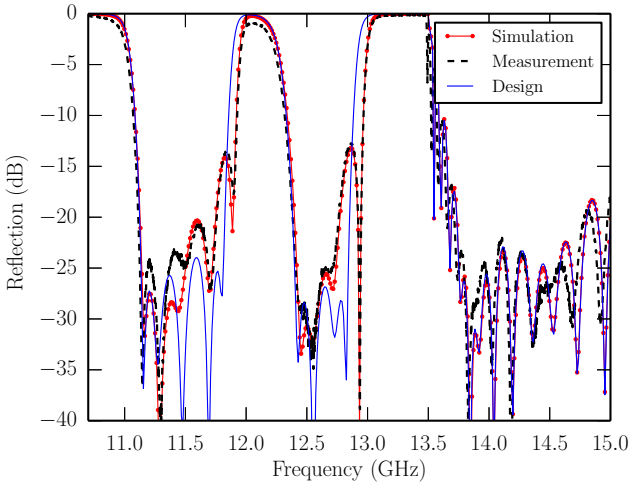

Fig. 11. Comparison between the original S_{11} designed response, simulation and measurement of the triplexer of Fig. 10.

return losses better than 25 dB over the bandwidth of the three filters. As shown in Fig. 8b, this solution is a slightly better option than our proposed methodology, but the differences between the two responses are certainly small. Furthermore, our proposed methodology is less CPU-intensive since, in each step, only one dimension is adjusted and the full-wave simulations are just performed at one frequency point (center frequency of the filter being adjusted).

Starting from the proposed initial response shown in Fig. 8, the conventional multiplexer design procedure described in [1] (sequential adjustment of filters until specifications are fulfilled) is applied. Without much effort, the final response depicted in Fig. 9 is obtained. In order to validate this design, the final response is compared with the simulation obtained with the commercial software tool Ansys' HFSS 15.

B. Ku-band triplexer for PIM measurement

This next example involves the design of a 26% relative-bandwidth triplexer. This triplexer is used as test bed for Passive Intermodulation (PIM) measurements at Ku-band. The specifications for the transmission (Tx) and reception (Rx) channels of the triplexer are as follows:

- Frequency bands:
  - Tx1 band: 11.15 GHz to 11.75 GHz
  - Tx2 band: 12.45 GHz to 12.75 GHz
  - Rx (PIM) band: 13.70 GHz to 14.55 GHz
- CPRL in band: 20 dB
- Rejection of Tx1 & Tx2 over Rx band: 80 dB
- Rejection of Rx over Tx1 & Tx2 band: 150 dB

The physical structure of this component is depicted in Fig. 10. It is composed of an inductive high-pass filter for the reception branch (placed in front of the common port), and two bandpass filters for the transmission channels using the Hybrid Folded Rectangular Waveguide (HFRW) topology [20], [21]. The coupling between adjacent resonators is implemented via capacitive windows in the top/bottom walls of the cavity. Inductive windows provide the necessary cross-coupling to implement transmission zeros in the PIM reception band. They are required to fulfill the rejection specifications.

The designed triplexer was manufactured and tested. The measured response, along with the designed one, can be seen in Fig. 11. The deviations in the measured response occurred mainly in the edges of the passbands. Fortunately, design margins had been added to the bandpass transmission filters in order to cope with manufacturing deviations. Due to the small degradations within the actual specified passbands, the component was accepted for the intended application.

The investigation of the discrepancy between the designed and measured response in Fig. 11 revealed that the design of the multiplexer was performed without reaching full convergence in the simulations. In particular, the T-junctions were not properly modeled. In order to obtain more accurate results, the simulation time required by conventional full-wave modal

techniques for the characterization of the T-junctions [22]–[24] increased dramatically. The reason is the existence of inductive effects, related to the cross-coupling windows in HFRW filters, in an essentially capacitive structure. The mutual interaction between the inductive and capacitive sections forces a full-wave representation involving a very high number of localized modes.

To solve this problem, and after applying a revisited version of the theory described in [25], a technique for the fast generation of the full-wave model of constant width/height blocks from the separate solution of LSE and LSM problems has been developed. By using this analysis technique, the measured response could be recovered without much effort (see the Simulation results shown in Fig. 11). Exploiting this formulation, the CPU time required for the accurate simulation of the whole multiplexer was 0.5 s per frequency point in an AMD FX-8320 Eight-core Processor, 3.5 GHz, 32 GB RAM. In contrast, using conventional modal techniques this time increased to 3 s per frequency point for rather accurate (although still not full convergent) results.

C. C-band quadruplexer for PIM measurement

The last example considers the design of a quadruplexer that covers practically the entire recommended band of the WR-229 waveguide. As in the previous example, this component is the key part of a PIM measurement set-up, in this case for operation at C-band. The specifications of this multiplexer are:

- Frequency bands:
  - Tx1 band: 3.4 GHz to 3.61 GHz
  - Tx2 band: 3.81 GHz to 3.98 GHz
  - Tx3 band: 4.13 GHz to 4.26 GHz
  - Rx (PIM) band: 4.5 GHz to 4.85 GHz
- CPRL in band: 20 dB
- Rejection of Tx1, Tx2 & Tx3 over Rx band: 165 dB
- Rejection of Rx over Tx1, Tx2 & Tx3 band: 160 dB

As it can be seen from the stringent specifications, the complexity of this design, in terms of bandwidth (36% overall, with filters of 3.6%, 4.9%, 6% and 8.3% relative bandwidth, after the inclusion of design margins) and rejection levels, is unprecedented in the technical literature for manifold-coupled multiplexers. Under these conditions, the use of a proper design methodology, like the one presented in this paper, is fundamental.

The Rx channel (inline with the manifold) has been implemented by a combination of a 5-pole band-pass filter and a long high-pass section of reduced width to meet the formidable rejection level required at the transmission band. In contrast with the example of Section III-B, the waveguide is twisted into the meandering block shown in Fig. 12 to compact the footprint of the design. Similarly, corrugated low-pass filters have been added to the output of the five-pole HFRW bandpass filters in channels Tx2 and Tx3 to ensure the 165 dB of isolation between them and the Rx channel. For channel Tx1, this was not necessary as its passband is the furthest from the Rx channel band.

The complete structure of the designed quadruplexer is depicted in Fig. 12. As it can be seen, the manifold is

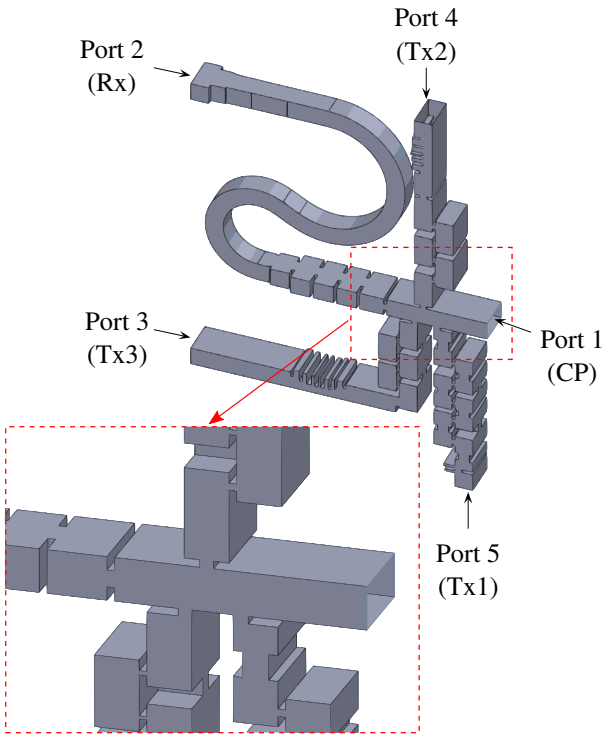

Fig. 12. Quadruplexer for PIM measurements at C-band. Detail of the manifold is included.

extremely short. In this example, the optimal distance between Tx2 and Tx3, obtained from the proposed interconnection procedure, is very close to $\lambda_g/2$. With the aim of minimizing the size of the manifold, a non-optimal but minimal separation is selected (see Fig. 4). This choice is troubling once Tx1 is connected to the manifold, since the physical separation between Tx1 and Tx3 is so small. Such a small gap between filters limits the amount of heat that can be dissipated in that area of the component and prevents the introduction of assembling screws. For that reason, the first coupling window of both of these filters is not centered with respect to the cavity, but shifted instead, to increase the gap between filters (this can be seen in the detail of Fig. 12).

The quadruplexer has been manufactured from aluminum using a tuning-less clam-shell assembly. The measured results are depicted in Fig. 13. A very good agreement can be seen between the designed response computed with FEST3D 6.8.6 and measurements. All the T-junctions of the manifold and the HFRW filters were efficiently modeled using the same analysis technique already developed and exploited for the example in subsection III-B. Due also to the efficient design technique proposed in this paper, which provides a good starting point after application of the fast algorithm for interconnecting the filters, it is possible to successfully carry out the design of such a large tuning-less multiplexer in reasonable CPU times. Note that no tuning has been performed on the multiplexer. As shown, return losses are better than 22.3 dB and insertion losses are smaller than 0.5 dB in all passbands. The rejection level has been successfully validated up to 150 dB, which was the limit of the measurement system due to undesired leakages between cables and instrumentation equipment.

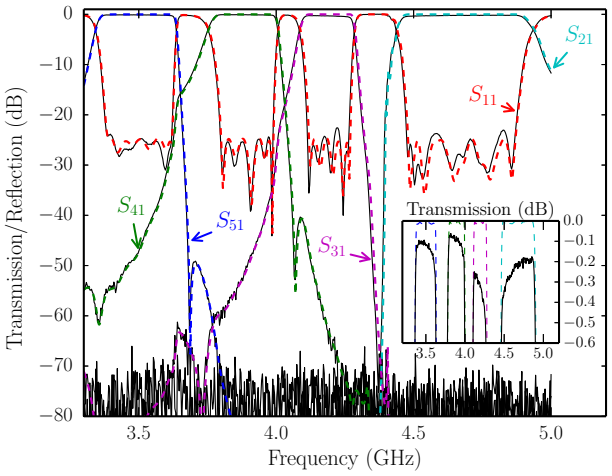

Fig. 13. Magnitude of the scattering parameters of the optimized quadruplexer for PIM measurements at C-band simulated with FEST3D 6.8.6. Dashed lines correspond to simulated results, whereas solid lines refer to measured results. Very good agreement can be seen between both sets of data. The transmission between the common port and the different channels is shown in the inset of the figure. As it can be seen, the insertion losses are better than 0.5 dB in all bands.

IV. Conclusion

In this paper, a systematic design methodology for wideband manifold-coupled multiplexers has been presented. Specific issues, associated with the design of multiplexers for wideband applications, have been tackled. In particular, the presence of unwanted peaks in the response has been mitigated by eliminating stubs (between the manifold and filters) and minimizing the length of the manifold. In addition, shorter manifolds without interconnecting stubs also produce lighter and more compact hardware solutions, which are always desirable features. Likewise, the interaction between adjacent filters is compensated during the first stages of the design by using an EM-driven design procedure. Filters are sequentially connected to the manifold and their interconnection adjusted to behave like the first inverter of each filter. This simple and fast methodology provides an adequate starting point for the successful optimization of wideband multiplexers.

Examples of designed multiplexers have been provided to validate the application of the design technique. Measurements from two manufactured prototypes have been included. A high degree of agreement between these measurements and simulations has been found.

Acknowledgment

The authors would like to thank Prof. Antonio Morini from Universita Politecnica delle Marche for the fruitful discussions on the efficient design of manifold-coupled multiplexers.

References

[1] R. J. Cameron and M. Yu, "Design of manifold-coupled multiplexers," *IEEE Microwave Magazine*, vol. 8, no. 5, pp. 46–59, Oct 2007.

[2] V. Boria, P. Soto, and S. Cogollos, "Distributed models for filter synthesis," *IEEE Microwave Magazine*, vol. 12, no. 6, pp. 87–100, Oct 2011.

[3] A. Atia, "Computer-aided design of waveguide multiplexer," *IEEE Trans. Microw. Theory Techn.*, vol. 22, no. 3, pp. 332–336, Mar 1974.

[4] J. Rhodes and R. Levy, "Design of general manifold multiplexers," *IEEE Trans. Microw. Theory Techn.*, vol. 27, no. 2, pp. 111–123, Feb 1979.

[5] M. Guglielmi, "Simple CAD procedure for microwave filters and multiplexers," *IEEE Trans. Microw. Theory Techn.*, vol. 42, no. 7, pp. 1347–1352, Jul 1994.

[6] R. Mansour, B. Jolley, V. Dokas, S. Ye, and F. Thomson, "Design of high power superconductive output multiplexers," in *Proc. 1996 IEEE MTT-S Int. Micr. Symp. Dig.*, vol. 3, June 1996, pp. 1485–1488 vol.3.

[7] M. Ismail, D. Smith, A. Panariello, Y. Wang, and M. Yu, "EM-based design of large-scale dielectric-resonator filters and multiplexers by space mapping," *IEEE Trans. Microw. Theory Techn.*, vol. 52, no. 1, pp. 386–392, Jan 2004.

[8] J. Montejo-Garai, J. Ruiz-Cruz, and J. Rebollar, "Full-wave design of H-plane contiguous manifold output multiplexers using the fictitious reactive load concept," *IEEE Trans. Microw. Theory Techn.*, vol. 53, no. 8, pp. 2628–2632, Aug 2005.

[9] Y. Wang, S. Li, and M. Yu, "Hybrid models for effective design and optimization of large-scale multiplexing networks," *IEEE Trans. Microw. Theory Techn.*, vol. 61, no. 5, pp. 1839–1849, May 2013.

[10] M. Brumos, S. Cogollos, M. Martinez, P. Soto, V. Boria, and M. Guglielmi, "Design of waveguide manifold multiplexers with dual-mode filters using distributed models," in *Proc. 2014 IEEE MTT-S Int. Micr. Symp. Dig.*, June 2014, pp. 1–4.

[11] L. Accatino, "Computer-aided design of a Ku-band antenna diplexer," in *Proc. 1993 European Microwave Conference (EuMC)*, Sept 1993, pp. 544–546.

[12] K.-L. Wu and W. Meng, "A direct synthesis approach for microwave filters with a complex load and its application to direct diplexer design," *IEEE Trans. Microw. Theory Techn.*, vol. 55, no. 5, pp. 1010–1017, May 2007.

[13] U. Rosenberg, A. Bradt, M. Perelshtein, and P. Bourbonnais, "Extreme broadband waveguide diplexer design for high performance antenna feed systems," in *Proc. 2010 European Microwave Conference (EuMC)*, Sept 2010, pp. 1249–1252.

[14] A. Morini, T. Rozzi, and M. Mongiardo, "Efficient CAD of wideband contiguous channel multiplexers," in *Proc. 1996 IEEE MTT-S Int. Micr. Symp. Dig.*, vol. 3, June 1996, pp. 1651–1654 vol.3.

[15] A. Morini, T. Rozzi, M. Farina, and G. Venanzoni, "A new look at the practical design of compact diplexers," *IEEE Trans. Microw. Theory Techn.*, vol. 9, no. 54, pp. 3515–3520, Sept 2006.

[16] H. Hu and K.-L. Wu, "Coping with spurious effects in full-wave electromagnetic design of a wide-band waveguide multiplexer," in *Proc. 2012 IEEE MTT-S Int. Micr. Symp. Dig.*, June 2012, pp. 1–3.

[17] M. Yu and Y. Wang, "Enhanced microwave multiplexing network," *IEEE Trans. Microw. Theory Techn.*, vol. 59, no. 2, pp. 270–277, Feb 2011.

[18] A. Morini, T. Rozzi, and M. Morelli, "New formulae for the initial design in the optimization of T-junction manifold multiplexers," in *Proc. 1997 IEEE MTT-S Int. Micr. Symp. Dig.*, vol. 2, June 1997, pp. 1025–1028 vol.2.

[19] J. Uher, J. Bornemann, and U. Rosenberg, *Waveguide components for antenna feed systems: theory and CAD*. Artech House, 1993.

[20] M. Guglielmi, "Hybrid folded rectangular waveguide filter," ESA Patent 624, 2014.

[21] C. Carceller, P. Soto, V. Boria, M. Guglielmi, and D. Raboso, "New folded configuration of rectangular waveguide filters with asymmetrical transmission zeros," in *Proc. 2014 European Microwave Conference (EuMC)*, Oct 2014, pp. 183–186.

[22] J. Rebollar, J. Esteban, and J. Page, "Fullwave analysis of three and four-port rectangular waveguide junctions," *IEEE Trans. Microw. Theory Techn.*, vol. 42, no. 2, pp. 256–263, Feb 1994.

[23] V. Boria, S. Cogollos, H. Esteban, M. Guglielmi, and B. Gimeno, "Efficient analysis of a cubic junction of rectangular waveguides using the admittance-matrix representation," *IEE Proc. Microw., Antennas, Propag.*, vol. 147, no. 6, pp. 417–422, Dec 2000.

[24] G. Conciauro, M. Guglielmi, and R. Sorrentino, *Advanced Modal Analysis - CAD Techniques for Waveguide Components and Filters*. John Wiley & Sons, 2000.

[25] H. Altschuler and L. Goldstone, "On network representations of certain obstacles in waveguide regions," *IRE Trans. Microw. Theory Techn.*, vol. 7, no. 2, pp. 213–221, April 1959.